

ASPECTS OF NEUTRINO PRODUCTION IN SUPERNOVAE

TODD A. THOMPSON*

*Department of Astrophysical Sciences
 Princeton University
 Peyton Hall — Ivy Lane
 Princeton, New Jersey, 08544 USA
 E-mail: thomp@astro.princeton.edu*

I discuss neutrino production in supernovae (SNe) and the detection of both Galactic core collapse events and the diffuse extra-galactic MeV neutrino background expected from the integrated history of star formation. In particular, I consider what processes might affect our expectations for both. I focus on “rapid” rotation, defined as leading to millisecond initial neutron star spin periods. Rotation affects the neutrino luminosity, the average neutrino energy, the duration of the Kelvin-Helmholtz cooling epoch, and the ratios of luminosities and average energies between neutrino species; it can strongly suppresses the $\bar{\nu}_e$ as well as ν_μ , $\bar{\nu}_\mu$, ν_τ , and $\bar{\nu}_\tau$ fluxes relative to ν_e . As a result, depending on the prevalence of rapid rotation in SN progenitors through cosmic time, this may affect predictions for the MeV neutrino background and the history of nucleosynthetic enrichment. I emphasize connections between the MeV neutrino background and tracers of the star formation rate density at high redshift in other neutrino and photon wavebands.

1. Introduction

When the iron core of a massive star collapses, the implosion is reversed at nuclear densities when nuclei dissociate into free nucleons. The equation of state stiffens dramatically, driving a bounce shockwave into the supersonic infalling outer core. The bounce shock stalls almost immediately as a result of neutrino losses, the ram pressure of the infalling material, and the dissociation of nuclei into free nucleons across the shock. After the shock stalls, a characteristic post-bounce accretion structure obtains that is quasi-steady-state. The hot (~ 10 MeV) newly-born “proto”-neutron star (PNS) has a

*Lyman Spitzer Jr. Fellow

neutrinosphere radius of ~ 80 km.^a Overlying the PNS is a subsonic accretion flow, bounded by the stalled stand-off shockwave at ~ 200 km. Just above the PNS is a cooling layer and beyond that a region of net neutrino heating (the “gain” region) provided by both accretion luminosity as the matter falling through the bounce shock is incorporated into the PNS and by core neutrino luminosity as the PNS cools and deleptonizes.

The revival of the shock to an energy of order 10^{51} ergs is the focus of supernova theory. Any mechanism for this revival must fundamentally rely on the transfer of gravitational binding energy to the post-shock mantle.

The “neutrino mechanism”^{1,2} employs neutrino interactions — primarily $\nu_e n \leftrightarrow p e^-$ and $\bar{\nu}_e p \leftrightarrow n e^+$ — to transfer binding energy to the shocked matter in the post-bounce epoch. With the standard suite of microphysics and a solution to the Boltzmann equation for all neutrino species, the neutrino mechanism fails in one spatial dimension; the stalled bounce shock remains trapped forever, accreting the overlying stellar progenitor.^{3–9} Although some models show that multi-dimensional effects might be necessary for success of the neutrino mechanism,^{10–13} recent calculations employing more sophisticated neutrino transport fail to explode¹⁴ — albeit marginally. In some cases, successes are obtained.¹⁵ However, the recent calculation of Ref. 16 suggests that energy deposition via neutrino interactions may be sub-dominant at late times with respect to acoustic heating generated by oscillations of the PNS generated by anisotropic accretion; the systematics of this new “acoustic” mechanism have yet to be elaborated. Many recent complimentary works focus on the stability of the shockwave and the post-shock material, and its importance for the mechanism.^{17–19}

Quite apart from the details of the explosion mechanism, the total energy budget dictating the character of neutron star birth is set by the gravitational binding energy of the neutron star:

$$E_{\text{bind}} \approx 3 \times 10^{53} M_{1.4}^2 R_{10}^{-1} \text{ ergs}, \quad (1)$$

where $M_{1.4} = M/1.4 M_\odot$ and $R_{10} = R/10 \text{ km}$ are the neutron star mass and radius, respectively. Theoretical models suggest^{20,21} and detection of neutrinos from SN 1987A confirm that a fraction of order unity of this energy is radiated in ~ 10 MeV neutrinos on the Kelvin-Helmholtz timescale $\tau_{\text{KH}} \sim 10 - 100 \text{ s}$, long with respect to the collapse and explosion timescales.

^aWhere the optical depth to ν_e neutrinos $\sim 2/3$, an energy- and time-dependent quantity.

Using these results, a number of studies have been made of the MeV neutrino background expected from SNe.^{22–24} Indeed, the constraints on the background from SuperK²⁵ have become tight enough that, for example, a total energy radiated in $\bar{\nu}_e$ neutrinos of $E_{\text{bind}}/3$ per SN with $\langle \varepsilon_{\bar{\nu}_e} \rangle > 20$ MeV is excluded.²⁴ Estimates of the background must assume the total neutrino energy radiated per neutrino species per SN, the average neutrino energy per species, and neutrino oscillation parameters. For light water detectors like SuperK the dominant detection mode is single-species ($\bar{\nu}_e p \rightarrow n e^+$) and because the cross section for this interaction is proportional to the neutrino energy squared the partitioning of energy, mixing, and the spectral shape are essential. The typical assumption is that the energy is partitioned equally between species, that the spectrum is thermal, and that the average energy is $\sim 10 - 20$ MeV.

Although the total energy budget (in all channels) per SN is dictated by equation (1), it is interesting to consider what processes might affect the best estimates of the diffuse neutrino background and the expected neutrino signal from the next Galactic SN at order unity. Potential processes are both microphysical and macrophysical/astrophysical. As an example of the former, it is possible that a change to the neutrino opacities or the equation of state for dense matter may alter the neutrino luminosity (L_ν) and average energy ($\langle \varepsilon_\nu \rangle$) during the cooling epoch, while the total energy radiated per SN is unaltered.²¹ Alternatively, as an example of astrophysical uncertainty, one may include the assumption of a universal IMF with constant (neutron-star-producing) SN rate per solar mass per year of star formation as a function of redshift, environment, and metallicity. In addition, there are a number of potential macrophysical effects that might modify our expectations at first order, including rapid rotation of the massive progenitor's iron core just before collapse.³²

Millisecond rotation of the PNS is interesting for several reasons. First, it changes L_ν and $\langle \varepsilon_\nu \rangle$ and their ratios between species. This strongly affects the neutrino signature of core collapse and it may affect nucleosynthesis in the inner SN ejecta by altering the ratio of the ν_e to $\bar{\nu}_e$ fluxes during explosion.^{26,27} Second, rapid rotation may be accompanied by more significant gravitational wave emission than non-rotating progenitors, thereby opening up a new channel of emission for a fraction of E_{bind} . Third, rapid rotation may affect the morphology and nucleosynthesis of the remnant.^{28,29} Finally, rapid rotation at birth has been theoretically motivated by the existence of magnetars. Ref. 30 argue that millisecond

rotation may be necessary for production of the very high magnetic field strengths ($\sim 10^{15}\text{G}$) inferred for the magnetar neutron star subclass. Although uncertain, simple estimates imply that $> 10\%$ of all SNe produce magnetars.³¹

In §2, I summarize results⁸ from a set of 1D simulations of core collapse, including rotation in a parameterized way, and I briefly discuss the implications of these models for neutrino detection. In §3 I discuss the neutrino background and its connection to other observable backgrounds.

2. Neutrinos from Rotating Core Collapse

Details of the models presented here are given in Ref. 8. A rotating 15M_\odot progenitor (model “E15A”) from Ref. 32 and a set of 11M_\odot progenitors from Ref. 33 with imposed initial rotation profiles are calculated. The imposed profile is taken to be $\Omega(r) = (2\pi/P_0)[1 + (r/R_\Omega)]^{-2}$, where $R_\Omega = 1000\text{km}$; thus, the iron core is in roughly solid-body rotation out to R_Ω . The 11M_\odot models span spin periods of $1 \lesssim P_0 \lesssim 10\text{s}$ — the former corresponding to near-, but sub-Keplerian rotation after collapse and the latter yielding results virtually indistinguishable from non-rotating models. The $\Omega(r)$ profile for the 15M_\odot model most resembles the $P_0 = 2\text{s}$ 11M_\odot progenitor (see Fig. 1 of Ref. 8).

Figure 1 shows L_ν and $\langle \varepsilon_\nu \rangle$ as a function of time after bounce for each of our rotating models. None of the models reach a centrifugal barrier and none explode. Higher initial rotation rates yield lower core temperatures after bounce for the PNS. On average, after ν_e breakout, this effect produces lower core L_ν and $\langle \varepsilon_\nu \rangle$ for shorter P_0 . The fractional differences in $\langle \varepsilon_\nu \rangle$ between the model with $P_0 = 1.25\text{s}$ and a non-rotating model 200 ms after bounce are approximately 15%, 17%, and 30% for ν_μ , $\bar{\nu}_e$, and ν_e , respectively. The same comparison for L_ν yields fractional differences of 75%, 63%, and 33% for L_{ν_μ} , $L_{\bar{\nu}_e}$, and L_{ν_e} , respectively. The difference in L_{ν_μ} at 100 ms after bounce between our slowest and fastest rotators is a factor of ~ 6 . Despite the fact that model E15A has rapid rotation, it has a much larger L_{ν_e} after breakout than, for example, the $P_0 = 2\text{s}$ 11M_\odot model, even though they have similar initial $\Omega(r)$ profiles. This is due to the extended density profile of model E15A relative to the 11M_\odot model and the associated larger accretion luminosity after bounce.

Figure 2 shows the ratio of L_{ν_e} and $\langle \varepsilon_{\nu_e} \rangle$ to L_ν and $\langle \varepsilon_\nu \rangle$ for each species as a function of time in each rotating model. The total luminosity in

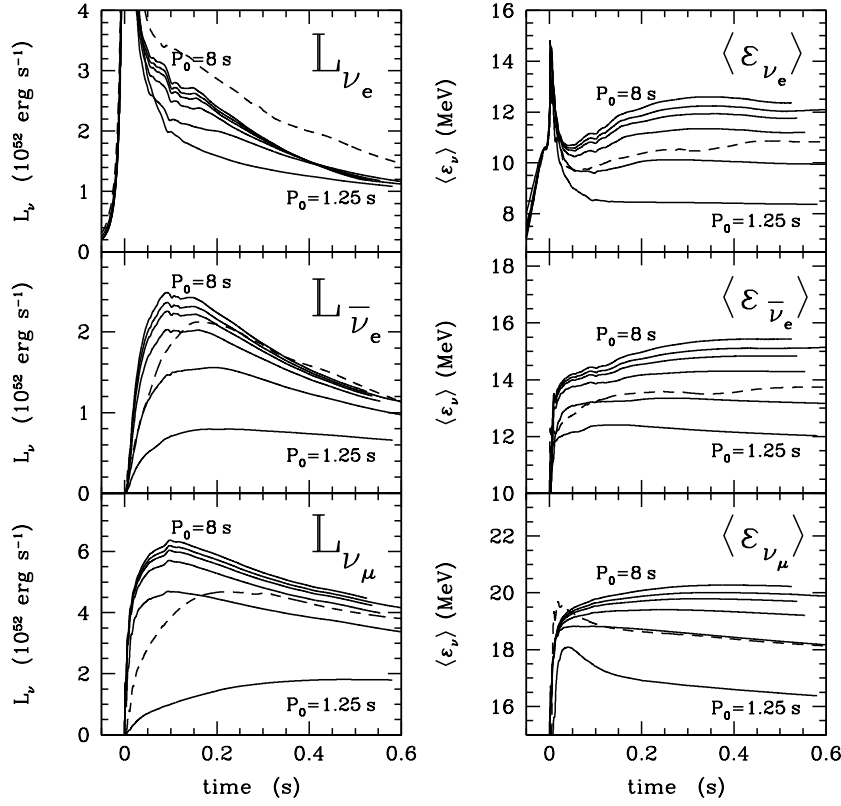
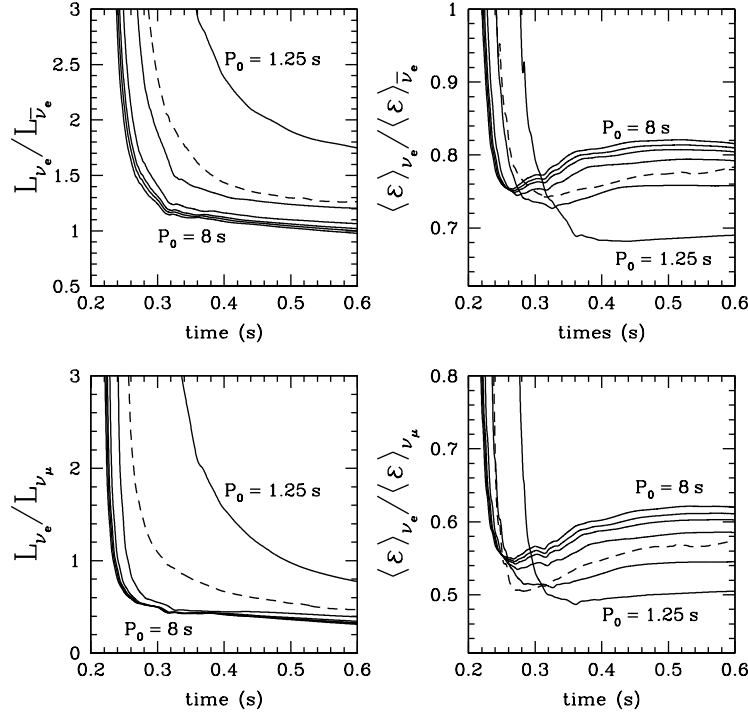


Figure 1. L_ν (left column) and $\langle \epsilon_\nu \rangle$ (right column) as a function of time after bounce for the $11 M_\odot$ progenitor with initial core spin periods of $P_0 = 1.25, 2, 3, 4, 5$, and 8 s (solid lines) and for the model E15A (dashed lines). 200 ms after bounce the lowest L_ν and $\langle \epsilon_\nu \rangle$ correspond to the shortest initial spin period. This hierarchy is preserved at all times and in all panels except in the case of L_{ν_e} 400 ms after bounce and at breakout. The ν_e breakout pulse is not shown in the upper-left panel. It is largest for the fastest rotator, with peak $L_{\nu_e} \sim 30\%$ larger than that for the slowest rotator ($\approx 2.4 \times 10^{53} \text{ ergs s}^{-1}$).

μ - and τ -type neutrinos, L_{ν_μ} , is suppressed by rapid rotation: for slow rotation ($P_0 = 8$ s) the ratio $L_{\nu_e}/L_{\nu_\mu} \approx 0.3$ at 0.5 s after bounce, whereas for $P_0 = 1.25$ s, $L_{\nu_e}/L_{\nu_\mu} \approx 0.8$. A similar enhancement of L_{ν_e} relative to $L_{\bar{\nu}_e}$ is also seen in the upper left panel. Although Figure 1 shows that $\langle \epsilon_{\nu_e} \rangle$ is decreased on average by rotation, the right panels here show that both $\langle \epsilon_{\bar{\nu}_e} \rangle$ and $\langle \epsilon_{\nu_\mu} \rangle$ are decreased yet more. The two upper panels may

Figure 2. Ratios of L_{ν} s (left column) and $\langle \epsilon_{\nu} \rangle$ s (right column) from Fig. 1.

be particularly important for the nucleosynthesis of inner ejecta in the gain region, should an explosion occur. Several studies address how the electron fraction and nucleosynthesis are determined by $L_{\nu_e}/L_{\bar{\nu}_e}$ and $\langle \epsilon_{\nu_e} \rangle / \langle \epsilon_{\bar{\nu}_e} \rangle$ as the explosion commences.^{26,27} A general study with these ratios motivated by Figure 2 may constrain the frequency of SN events with rapid rotation.

Figure 3 shows L_{ν} and $\langle \epsilon_{\nu} \rangle$ at 0.5 s after bounce for the 11 M_{\odot} progenitor as a function of P_0 . In the effectively non-rotating case $P_0 = 8$ s, $L_{\nu_e} : L_{\bar{\nu}_e} : L_{\nu_\mu}/4 :: 1 : 1.1 : 0.95$. As Figure 3 makes clear, this equality between neutrino species does not persist when rotation is rapid; for $P_0 = 1.25$ s, $L_{\nu_e} : L_{\bar{\nu}_e} : L_{\nu_\mu}/4 :: 1 : 0.6 : 0.4$. Although not explored systematically as a function of P_0 , multi-D simulations of rotating collapse also exhibit suppression of $\bar{\nu}_e$ and ν_μ at the level described here.^{34,35}

The strong suppression of both the $\bar{\nu}_e$ and ν_μ luminosity and average

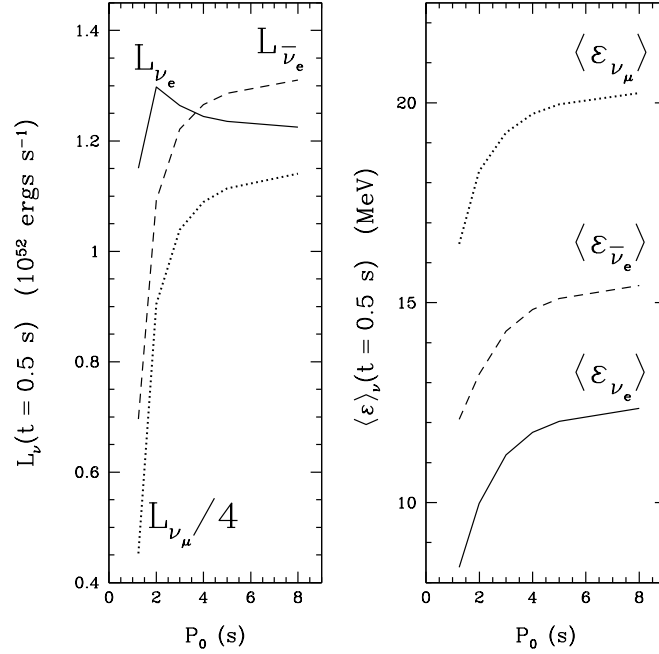


Figure 3. L_ν and $\langle \epsilon_\nu \rangle$, at $t = 0.5$ s after bounce, as a function of P_0 (see Figs. 1 & 2). Although L_{ν_e} is fairly constant, $L_{\bar{\nu}_e}$ and L_{ν_μ} decrease sharply with more rapid initial core rotation.

energy is important for the detection of neutrinos from the next Galactic SN. Figure 4 shows the integrated number of events expected in SuperK from the $11 M_\odot$ progenitors with $P_0 = 8$ s and 1.25 s at a distance of 10 kpc from the interactions $\bar{\nu}_e p \rightarrow n e^+$ and $\nu_e e^- \rightarrow \nu'_e e'^-$. Neutrino oscillations within the SN progenitor envelope, while the neutrinos are in transit, or within the Earth are neglected. The number rate of neutrinos detected is $\dot{N} \propto [L_\nu / \langle \epsilon_\nu \rangle] \sigma$, where σ is the cross section. Because $\sigma \propto \langle \epsilon_{\nu_e} \rangle$ for inelastic $\nu_e - e^-$ scattering and because L_{ν_e} is roughly independent of P_0 (Fig. 3), the total number of $\nu_e - e^-$ scattering events in SuperK is approximately independent of P_0 , although the ν_e breakout burst is somewhat larger in the rapidly rotating case, $P_0 = 1.25$ s. However, the dominant charged-current interaction $\bar{\nu}_e p \rightarrow n e^+$ has $\sigma \propto \langle \epsilon_{\bar{\nu}_e}^2 \rangle$ so that for this process $\dot{N} \propto L_{\bar{\nu}_e} \langle \epsilon_{\bar{\nu}_e} \rangle$. Thus, the strong decrease in both $L_{\bar{\nu}_e}$ and $\langle \epsilon_{\bar{\nu}_e} \rangle$ with P_0 (Fig. 3) leads to a very large decrease in $N(< t)$: 0.5 s after bounce the ratio between the total number of neutrino events for the two models is $\approx 1190/350 \approx 3.4$.

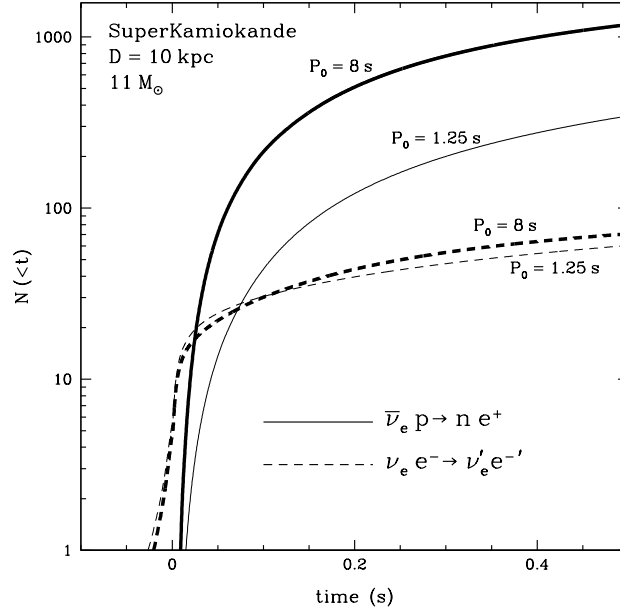


Figure 4. Integrated number of events in SuperK $N(< t)$ for a SN at 10 kpc as a function of time after bounce. Only the $P_0 = 8\text{s}$ (*heavy lines*) and $P_0 = 1.25\text{s}$ (*thin lines*) models are shown. Event rates for the reactions $\nu_e e^- \rightarrow \nu'_e e^-$ (*dashed lines*) and $\bar{\nu}_e p \rightarrow n e^+$ (*solid lines*) are shown separately. In the rapidly rotating model the $\bar{\nu}_e$ signal is strongly suppressed and the prompt ν_e signal persists for $\approx 0.05\text{s}$ before being swamped by the $\bar{\nu}_e$ s, much longer than for the $P_0 = 8\text{s}$ model.

3. The Energy Budget of the Universe

A simple estimate for the contribution of SNe to the MeV neutrino background can be made by relating the total energy expected in neutrinos from each SN to the star formation rate, \dot{M}_\star , which is related to the total IR luminosity ($L_{\text{TIR}} [8 - 1000]\mu\text{m}$) by $L_{\text{TIR}} = \epsilon \dot{M}_\star c^2$, where ϵ is an IMF-dependent constant. Assuming that the SN rate per unit star formation Γ_{SN} is a constant fraction of \dot{M}_\star and that the total energy radiated is $E_\nu^{\text{tot}} = 10^{53.5}$ ergs per SN, one finds that (averaging over a suitably large number of systems or time)

$$L_\nu \approx 3L_{\text{TIR}} E_{53.5} \beta_{17}, \quad (2)$$

where L_ν is the total neutrino luminosity and $\beta_{17} = (\Gamma_{\text{SN}}/\epsilon)/17M_\odot$ has only a weak dependence on the assumed IMF because massive stars dom-

inate photon and neutrino production. The total specific intensity in MeV SN neutrinos expected from the star formation history of the universe can then be scaled from the integral over the comoving star formation rate density as a function of redshift, $\dot{\rho}_*(z)$. Taking $\Omega_m = 0.3$ and $\Omega_\Lambda = 0.7$ and using “RSF2” for $\dot{\rho}_*(z)$ from Ref. 36, one finds that $\zeta = \int dz [\dot{\rho}_*(z)/\dot{\rho}_*(z=0)] / \{(1+z)^2 [\Omega_m(1+z)^3 + \Omega_\Lambda]^{1/2}\} \approx 2$. Thus,

$$F_\nu^{\text{tot}} \sim 4 (\zeta/2) \ 10 \text{ MeV cm}^{-2} \text{ s}^{-1} \text{ sr}^{-1}, \quad (3)$$

where $H_0 = 71 \text{ km s}^{-1} \text{ Mpc}^{-1}$ has been assumed and the dependences on E_ν^{tot} and β have been dropped. The dominant reaction for detection of relic neutrinos in SuperK is $\bar{\nu}_e p \rightarrow n e^+$. Assuming that $F_{\bar{\nu}_e} \approx F_\nu^{\text{tot}}/6$, $\langle \varepsilon_{\bar{\nu}_e} \rangle \approx 15 \text{ MeV}$, and accounting for the fact that SuperK’s sensitivity to the diffuse background is maximized for $\varepsilon_{\bar{\nu}_e} \sim 20 \text{ MeV}$, considerably larger than $\sim 15/(1+z) \text{ MeV}$ for $z \approx 1$, one finds an event rate in SuperK of $\sim 1 \text{ yr}^{-1}$, in accord with more complete estimates.^{22–24} As Figures 3 & 4 make clear, if a large fraction of all SNe are born rapidly rotating, then the background estimate is significantly decreased because of the strong decrease in $\langle \varepsilon_{\bar{\nu}_e} \rangle$ and $\langle \varepsilon_{\bar{\nu}_\mu} \rangle$ with decreasing P_0 .

As implied by equations (2) and (3), the massive stars that generate MeV neutrinos also produce a corresponding total IR background of $F_{\text{TIR}}^{\text{tot}} \approx 2 \times 10^{-5} \text{ ergs cm}^{-2} \text{ s}^{-1} \text{ sr}^{-1} \approx 20 \text{ nW m}^{-2} \text{ sr}^{-1}$. The SNe that accompany this star formation also accelerate cosmic ray electrons and protons to very high energies. Inelastic collisions between cosmic ray protons and gas in the ISM of star-forming galaxies produce $\pi^{+,-}$ and π^0 , which subsequently decay to $e^{-,+}$ and high-energy neutrinos, and γ -rays, respectively. The primary electrons and secondary electrons/positrons suffer synchrotron losses in the host galactic magnetic field. Inverse Compton and bremsstrahlung losses likely also contribute significantly to cooling.³⁷ The observed tight linear correlation between the IR and radio luminosity of star-forming and starburst galaxies implies that the contribution to the IR background from star formation comes together with radio emission at the level $\nu I_\nu(\text{radio}) \approx 3 \times 10^{-11} \text{ ergs cm}^{-2} \text{ s}^{-1} \text{ sr}^{-1}$, assuming a flat cosmic ray spectrum — consistent with $\sim 5\%$ of the 10^{51} ergs of asymptotic kinetic energy of each SN going into cosmic rays.³⁸ Recent work suggests that inelastic $p-p$ collisions in the dense ISM of starburst galaxies may contribute significantly to the diffuse GeV γ -ray and GeV–TeV ν_μ -neutrino background at the level of $\sim 10^{-7} \text{ GeV cm}^{-2} \text{ s}^{-1} \text{ sr}^{-1}$.^{38,39} Thus, stars that produce SNe may dominate — or contributor importantly to — the neutrino (MeV & GeV–TeV), γ -ray, IR, and radio backgrounds.

Acknowledgments

I thank Adam Burrows, Eliot Quataert, and Eli Waxman for collaboration and many stimulating conversations.

References

1. Bethe, H. & Wilson, J. R. 1985, ApJ, 295, 14
2. Janka, H.-Th. 2001, A&A, 368, 527
3. Rampp, M., & Janka, H.-T. 2000, ApJL, 539, L33
4. Rampp, M., & Janka, H.-T. 2002, A&A, 396, 361
5. Mezzacappa, A., et al. 2001, PRL, 86, 1935
6. Liebendörfer, M., et al. 2001, PRD, 63, 103004
7. Thompson, T. A., Burrows, A., & Pinto, P. A. 2003, ApJ, 592, 434
8. Thompson, T. A., Quataert, E., & Burrows, A. 2005, ApJ, 620, 861
9. Sumiyoshi, K., et al. 2005, ApJ, 629, 922
10. Herant, M., et al. 1994, ApJ, 435, 339
11. Burrows, A., Hayes, J., & Fryxell, B. A. 1995, ApJ, 450, 830
12. Janka, H.-T., & Mueller, E. 1996, A&A, 306, 167
13. Fryer, C. L. 1999, ApJ, 522, 413
14. Buras, R., et al. 2003, PRL, 90, 241101
15. Buras, R., et al. 2006, A&A, 447, 1049
16. Burrows, A., et al. 2006, ApJ, 640, 878
17. Blondin, J. M., Mezzacappa, A., & DeMarino, C. 2003, ApJ, 584, 971
18. Ohnishi, N., Kotake, K., & Yamada, S. 2006, ApJ, 641, 1018
19. Foglizzo, T., et al. 2006, arXiv:astro-ph/0606640
20. Burrows, A. & Lattimer, J.M. 1986, ApJ, 307, 178
21. Pons, J. A., et al. 1999, ApJ, 513, 780
22. Ando, S. & Sato, K. 2002, Prog. Theoretical Phys., 107, 957
23. Strigari, L. E., et al. 2005, JCAP, 4, 17
24. Yuksel, H., Ando, S., & Beacom, J. 2005, arXiv:astro-ph/0509297
25. Malek, M., et al. 2003, PRL, 90, 061101
26. Pruet, J., et al. 2005, ApJ, 623, 325
27. Fröhlich, C., et al. 2006, ApJ, 637, 415
28. Thompson, T. A., Chang, P., & Quataert, E. 2004, ApJ, 611, 380
29. Bucciantini, N., et al. 2006, MNRAS, 368, 1717
30. Duncan, R. C., & Thompson, C. 1992, ApJL, 392, L9
31. Woods, P. M., & Thompson, C. 2004, arXiv:astro-ph/0406133
32. Heger, A., Langer, N., & Woosley, S. E. 2000, ApJ, 528, 368
33. Woosley, S. E. & Weaver, T. A. 1995, ApJS, 101, 181
34. Fryer, C. L., & Heger, A. 2000, ApJ, 541, 1033
35. Dessart, L., et al. 2006, ApJ, 644, 1063
36. Porciani, C., & Madau, P. 2001, ApJ, 548, 522
37. Thompson, T. A., et al. 2006, ApJ, 645, 186
38. Thompson, T. A., Quataert, E., & Waxman, E. 2006, arXiv:astro-ph/0606665
39. Loeb, A., & Waxman, E. 2006, JCAP, 5, 3